Exploration of Group Index for Silicon Mach-Zehnder Interferometers

Maryann C. Tung, edX: mtungsten
maryann.tung@gmail.com

I. Introduction

Fast propagation speed and high bandwidth make photonics an attractive choice for emerging computing applications, such as artificial intelligence and quantum computing. As new waveguide materials and designs are being tested, it is critical to evaluate their performance, including how quickly light propagates through them. One key indicator for this is group index, which can be used to find the velocity at which optical pulses travel through the fabricated waveguide.

In this project, we find the group index for silicon (Si) waveguides patterned using electron-beam lithography by fabricating imbalanced Mach-Zehnder Interferometers (MZIs). The fabricated MZIs all have the same materials, fabrication process, and waveguide shape – the only difference is the change in waveguide path length (ΔL). As a result, we expect different MZI structures to yield similar group indices, allowing us to confirm the group index for these waveguides across multiple structures.

II. Theory

In a Mach-Zehnder Interferometer, light from a single source is split into two separate waveguides and then recombined. By adjusting the relative phase of the light in the two waveguide branches, it is possible to vary the output beam intensity from full intensity to no intensity using constructive and destructive interference. Here, we implement an MZI using a y-branch splitter and a y-branch combiner connected by waveguides of difference lengths to induce a phase difference (see Figure 1) between the waveguide branches. The output light intensity (I_o) for this structure is

$$I_o = \frac{I_i}{4}\left|e^{-i\beta_1 L_1 - \frac{\alpha_1}{2}L_1} + e^{-i\beta_2 L_2 - \frac{\alpha_2}{2}L_2}\right|^2 \quad (1),$$

where I_i is the input light intensity, $L_{1,2}$ are the lengths of the waveguide branches, $\beta_{1,2}$ are the propagation constants of light through the waveguides, and $\alpha_{1,2}$ are the attenuation factors for the branches. Assuming identical and lossless waveguides, we can simplify Equation (1) as follows:

$$I_o = \frac{I_i}{2}[1 + \cos(\beta \Delta L)] \quad (2),$$

where ΔL is the path length difference between the two MZI branches.

Fig. 1. Diagram of an imbalanced Mach-Zehnder Interferometer. In this device, the light comes in from the left-hand y-branch splitter, splits between the two waveguide arms, and then recombines at the output y-branch combiner. Figure modified from [1].

To calculate the group index for this structure, we can check the spacing of adjacent valleys in the output intensity spectrum, called the free spectral range (FSR). Given the wavelength (λ) of the input light and the waveguide path length difference, we can use the following to solve for the group index (n_g):

$$FSR = \lambda^2 / \Delta L n_g \quad (3).$$

After fabricating the MZIs, we will measure the output intensity spectrum as a function of wavelength, extract the FSR, and use the FSR to calculate the group index. We will then compare the group index calculated from the device measurements with simulations of equivalent devices to evaluate the level of non-ideality in the fabricated devices.

III. Modeling and Simulation

To simulate the fabricated circuits, we used MODE to model the Si waveguides and INTERCONNECT to model the full MZI circuits. In both cases, we based the models on our fabricated devices with the design parameters given in Table 1. Starting with the Lumerical MODE simulation, we checked the confinement of the fundamental TE optical mode for the Si waveguides. Figure 2-a shows the optical mode for the straight portion of the waveguide at λ = 1550 nm, and Figure 2-b shows the optical mode at the bend for the same wavelength. In both cases, the optical mode is well-confined to the Si core, indicating that the bend radius is sufficiently large to prevent excess loss due to radiation at the bend.

Table 1: Waveguide Model Parameters	
Core Material	Si
Cladding Material	SiO_2
Waveguide Width	500 nm
Waveguide Height	220 nm
Bend Radius	5 μm
Operating Wavelength	1550 nm
Polarization	TE

In addition to visualizing the optical mode, we also used Lumerical MODE to model effective index (n_{eff}) and group index (n_g). Figures 3 and 4 show both parameters as a function of wavelength. Fitting the plot of n_{eff} vs λ with a Taylor expansion, we found the compact model of the waveguide:

$n_{eff} = 2.45 - 1.13(\lambda - 1.55) - 0.042(\lambda - 1.55)^2$ (4),

where λ has the units of microns.

Next, we modeled the fabricated MZI circuits in INTERCONNECT with the circuit model illustrated in Figure 5. In Figure 6, the layout of the full set of fabricated MZIs is drawn, along with the length of the waveguides connecting the y-branch splitter to the y-branch combiner for each circuit. For each of the seven MZIs, we plotted gain as a function of wavelength (see Figure 7) and extracted the free spectral range at $\lambda \approx 1550$ nm (see Table 2). Using Equation (3), we calculated n_g for each extracted FSR value. As seen in Table 2, we found good agreement between the n_g values derived from MODE and INTERCONNECT, with the n_g value from MODE falling <1% below those from INTERCONNECT.

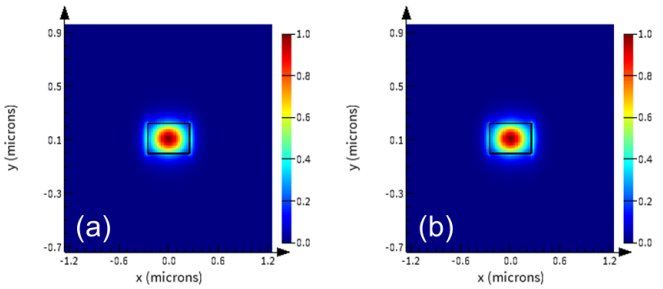

Fig. 2. Lumerical MODE simulations of optical mode for the fabricated Si waveguides (a) without a bend and (b) with a bend. See Table 1 for the simulation parameters. The mode depicted here is the fundamental mode, which 99% TE polarized.

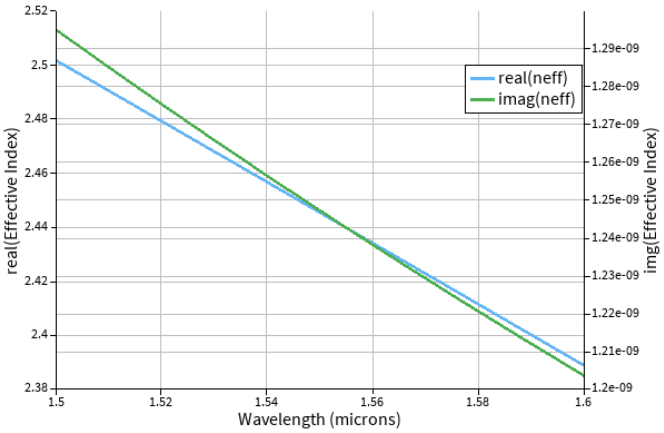

Fig. 3. Lumerical MODE simulation of the real (blue line) and imaginary (green line) components of the effective index for the fabricated Si waveguides.

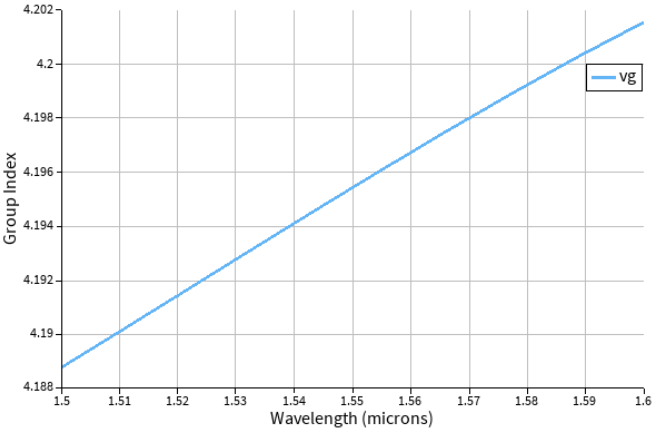

Fig. 4. Lumerical MODE simulation of the group index for the fabricated Si waveguides.

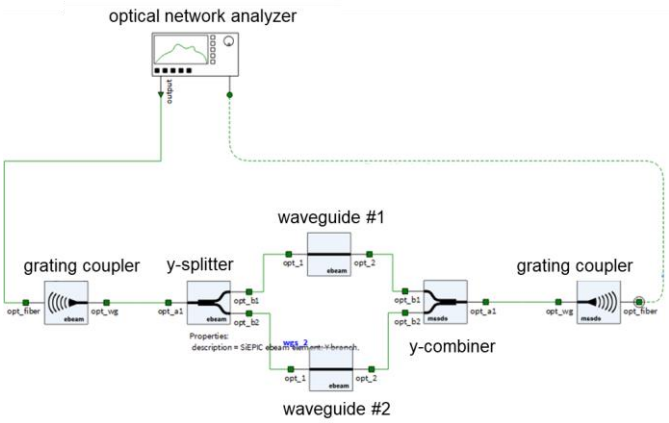

Fig. 5. Lumerical INTERCONNECT circuit used to simulate the fabricated MZIs. The components used for the simulation were taken from the SiEPIC design kit [2, 3].

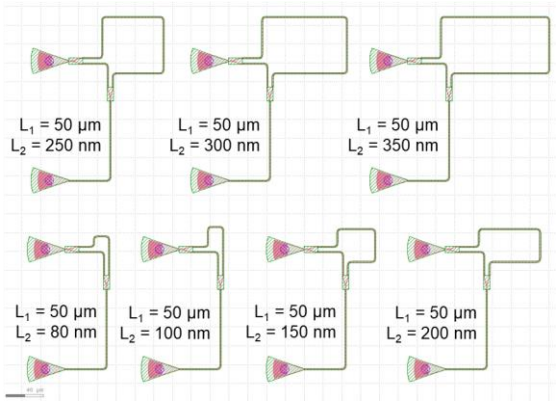

Fig. 6. Layout of the fabricated MZI circuits, showing the lengths L_1 and L_2 of waveguide #1 and waveguide #2, respectively, from Figure 5.

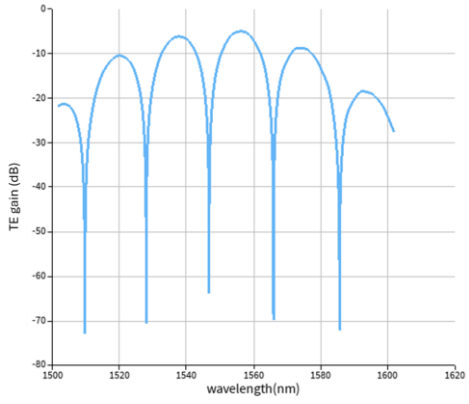

Fig. 7. Example plot of gain vs wavelength, as simulated in Lumerical INTERCONNECT. Here, gain is shown for an MZI with L_1 = 50 nm and L_2 = 80 nm.

Table 2: FSR & n_g for Simulated MZIs			
L_1 [µm]	L_2 [µm]	FSR [nm]	n_g
50	80	18.89	4.24
50	100	11.32	4.24
50	150	5.63	4.27
50	200	3.80	4.21
50	250	2.84	4.23
50	300	2.26	4.25
50	350	1.90	4.21

IV. Fabrication

The set of MZI devices illustrated in Figure 6 were fabricated and measured using the methodology given in [4]: "The photonic devices were fabricated using the NanoSOI MPW fabrication process by Applied Nanotools Inc. (http://www.appliednt.com/nanosoi; Edmonton, Canada) which is based on direct-write 100 keV electron beam lithography technology. Silicon-on-insulator wafers of 200 mm diameter, 220 nm device thickness and 2 µm buffer oxide thickness are used as the base material for the fabrication. The wafer was pre-diced into square substrates with dimensions of 25 x 25 mm, and lines were scribed into the substrate backsides to facilitate easy separation into smaller chips once fabrication was complete. After an initial wafer clean using piranha solution (3:1 H_2SO_4:H_2O_2) for 15 minutes and water/IPA rinse, hydrogen silsesquioxane (HSQ) resist was spin-coated onto the substrate and heated to evaporate the solvent. The photonic devices were patterned using a JEOL JBX-8100FS electron beam instrument at The University of British Columbia. The exposure dosage of the design was corrected for proximity effects that result from the backscatter of electrons from exposure of nearby features. Shape writing order was optimized for efficient patterning and minimal beam drift. After the e-beam exposure and subsequent development with a tetramethylammonium sulfate (TMAH) solution, the devices were inspected optically for residues and/or defects. The chips were then mounted on a 4" handle wafer and underwent an anisotropic ICP-RIE etch process using chlorine after qualification of the etch rate. The resist was removed from the surface of the devices using a 10:1 buffer oxide wet etch, and the devices were inspected using a scanning electron microscope (SEM) to verify patterning and etch quality. A 2.2 µm oxide cladding was deposited using a plasma-enhanced chemical vapour deposition (PECVD) process based on tetraethyl orthosilicate (TEOS) at 300ºC. Reflectometry measurements were performed throughout the process to verify the device layer, buffer oxide and cladding thicknesses before delivery."

Table 4: Group Index and Effective Index Values for Simulated Waveguides			
Waveguide Dimensions		n_g	n_{eff}
w = 470 nm	t = 210 nm	4.240	2.3526
	t = 225 nm	4.259	2.4112
w = 550 nm	t = 210 nm	4.108	2.4758
	t =225 nm	4.123	2.5330

"To characterize the devices, a custom-built automated test setup [1, 5] with automated control software written in Python was used [6]. An Agilent 81600B tunable laser was used as the input source and Agilent 81635A optical power sensors as the output detectors. The wavelength was swept from 1500 to 1600 nm in 10 pm steps. A polarization maintaining (PM) fibre was used to maintain the polarization state of the light, to couple the TE polarization into the grating couplers [7]. A 90º rotation was used to inject light into the TM grating couplers [7]. A polarization maintaining fibre array was used to couple light in/out of the chip [8]."

V. Experiment Data & Analysis

After measuring the fabricated MZIs, the free spectral range (FSR) was extracted from each transmission spectrum. Table 3 gives the extracted FSR values for both sets of devices, as well as the group index calculated from the average FSR for each MZI design. The extracted FSR values from the two device sets show good agreement (within 1-4%), indicating no major die-to-die fabrication variations. Similarly, the group index is similar across the devices, with an average n_g of 4.123 with a standard deviation of 0.087. The group index for the devices with $\Delta L = 150$ µm deviate the most from the rest of the devices, suggesting a possible error in the MZI design. For the $\Delta L = 150$ µm MZI design, a change of ~3% in the ΔL between the two MZI branches could account for the variation in change in group index. Similarly, the way the waveguide bends are implemented in that MZI design could cause poorer optical confinement, also leading to a lower group index.

To better understand the deviation in the performance in the manufactured devices from the designed devices, we performed a corner analysis for waveguides with widths 470 - 550 nm and

Table 3: Free Spectral Range and Group Index for Measured Devices								
		MZI ΔL						
		30 µm	50 µm	100 µm	150 µm	200 µm	250 µm	300 µm
FSR	Set 1	19.24	11.60	5.79	4.03	2.85	2.29	1.92
	Set 2	19.35	11.46	5.87	4.08	2.95	n/a*	1.92
	% Difference	0.6%	-1.2%	1.4%	1.2%	3.4%	n/a	0.0%
	Average	19.30	11.53	5.83	4.06	2.90	2.29	1.92
n_g	Average	4.15	4.17	4.12	3.95	4.14	4.20	4.17

*Value missing due to measurement error

Table 5: Free Spectral Range Values for Simulated Devices								
		MZI ΔL						
Waveguide Dimensions		30 μm	50 μm	100 μm	150 μm	200 μm	250 μm	300 μm
w = 470 nm	t = 210 nm	18.066	11.261	5.611	3.765	2.821	2.240	1.879
	t = 225 nm	17.848	11.085	5.623	3.757	2.796	2.256	1.876
w = 550 nm	t = 210 nm	18.999	11.570	5.839	3.894	2.925	2.341	1.955
	t =225 nm	18.464	11.285	5.856	3.872	2.912	2.333	1.938

thicknesses 210 - 225 nm. Starting with the model of the different waveguide geometries in Lumerical MODE, we found the group and effective indices for each of the corner geometries (see Table 4). Next, we used the waveguide model from MODE to find the free spectral range for each MZI design in Lumerical INTERCONNECT (see Table 5). As shown in Figure 8, the group indices calculated from the measured MZIs fall closer to the lower bound of the corner analysis, suggesting that the fabricated waveguides may be thinner and wider than designed.

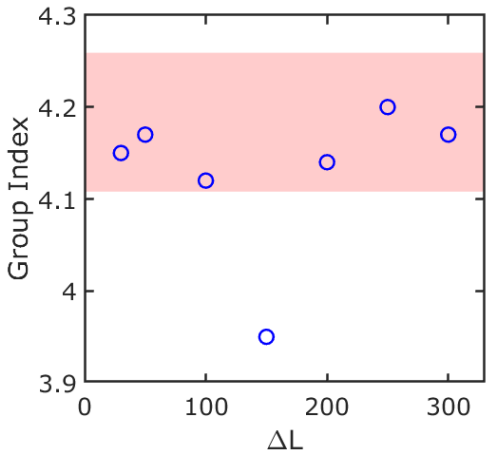

Fig. 8. Average group index for each fabricated MZI design (blue dots). The shaded red band shows the range of group index values simulated in Lumerical MODE for the corner waveguide geometries, with the upper limit showing n_g for the w = 470 nm and t = 225 nm waveguide and the lower limit showing n_g for the w = 550 nm and t = 210 nm waveguide.

Conclusion

In this work, we designed a set of imbalanced Mach-Zehnder Interferometers with varying path length differences between the two branches. We modeled these devices in Lumerical MODE and INTERCONNECT to predict their group index and free spectral range. After fabricating the devices, we measured the transmission spectra and extracted the free spectral range and group index values for each device. Comparing the measured and simulated devices, the group index for the measured devices was smaller than the simulated group index, suggesting that the geometry of the fabricated waveguides differ from the design. Based on a corner analysis, it appears likely that the fabricated waveguides are thinner and wider than designed, although cross-sections of the waveguides would be needed to confirm the exact geometry.

References

[1] L. Chrostowski and M. Hochberg, *Silicon Photonics Design*, Glasgow, United Kingdom: Bell and Bain Ltd., 2015, ch. 4, pp. 92-159.

[2] L. Chrostowski et al., "Design and simulation of silicon photonic schematics and layouts," *Proc. SPIE*, vol. 9891, no. 989114, May 2016, doi: 10.1117/12.2230376.

[3] L. Chrostowski et al., "Silicon Photonic Circuit Design Using Rapid Prototyping Foundry Process Design Kits," *IEEE Journal of Selected Topics in Quantum Electronics*, vol. 25, no. 5, May 2019, doi: 10.1109/JSTQE.2019.2917501.

[4] L. Chrostowski, "Final Report – Details," in *Silicon Photonics Design, Fabrication and Data Analysis*, 2025, edX.

[5] http://mapleleafphotonics.com, Maple Leaf Photonics, Seattle WA, USA.

[6] http://siepic.ubc.ca/probestation, using Python code developed by Michael Caverley.

[7] Y. Wang et al., "Focusing sub-wavelength grating couplers with low back reflections for rapid prototyping of silicon photonic circuits," *Optics Express*, vol. 22, no. 17, pp. 20652-20662, 2014, doi: 10.1364/OE.22.020652.

[8] www.plcconnections.com, PLC Connections, Columbus OH, USA.